Electronic Supplementary Material (ESI) for Soft Matter.

Supporting Information

Isostructural Softening of the Filler Network in SBR/Silica Nanocomposites

Hoang Giang Trinh, Marlène Desloir, Fabien Dutertre, Jean-Charles Majesté, Florent Dalmas and Guilhem P. Baeza

guilhem.baeza@insa-lyon.fr

1. Thermogravimetric Analysis

We present in Figure S1, thermogravimetric experiments showing a good agreement between the nominal and the actual filler fraction in the whole set of nanocomposites. Note that in Table 1 (main text), the volume fractions are calculated from the density of the SBR and the silica such as $\rho_{SBR} = 0.94\ g\ cm^{-3}$ and $\rho_{silica} = 2.20\ g\ cm^{-3}$. In Figure S1a, the first drop of the mass (inset) is related with the amount of water adsorbed at the silica surface (growing with Φ_{si}). The loss of mass situated around 450 °C corresponds with the vaporization of the SBR. Figure S1b reveals a slightly faster degradation most likely related with the concentration of short PPG.

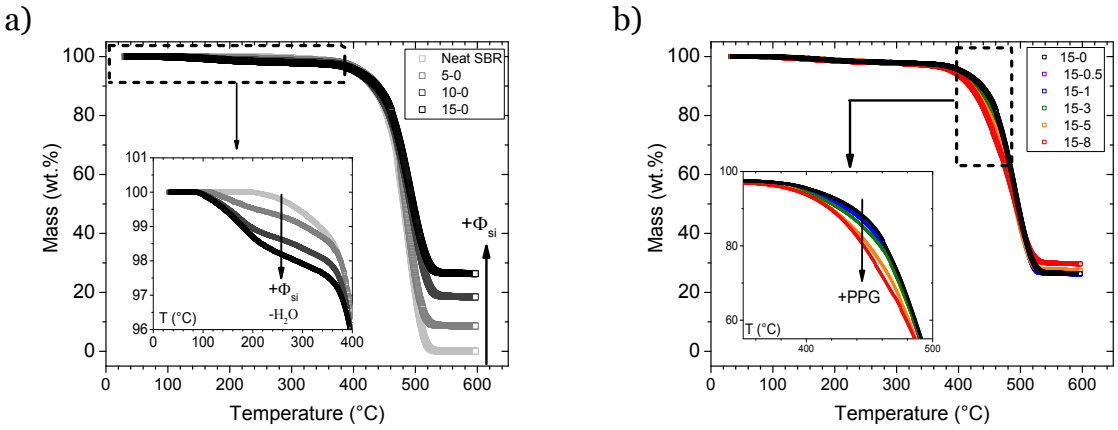

Figure S1: Thermogravimetric analysis performed on nanocomposites. a) Neat SBR matrix and PPG free nanocomposites loaded with 5, 10 and 15 vol.% in silica. Inset: zoom-in the region corresponding to the adsorbed water evaporation. b) Nanocomposites loaded with 15 vol.% in silica and various amount of PPG. Inset: zoom-in the region in which the PPG chains are likely to start their degradation.

2. Mastercurves building

The LVE characterization presented in Figure 3 (main text) is based on the time temperature superposition performed at low and high temperatures respectively for DMA and rheology experiments. We provide in Figure S2 the corresponding shift factors obtained for the Neat SBR and the 15-3 sample. A similar procedure has been used for all the nanocomposites. Remarkably, no vertical shift was required to build each piece of the mastercurves (DMA and rheology). We believe that this unexpected result is due to the good dispersion achieved through the use of the *Roller* rotors during the mixing procedure. Note that it was impossible to build such mastercurves for a slightly different silica (Zeosil 1165 MP) and *Banbury* rotors.[1] However, we used a vertical shift to "stick" together the DMA and the rheology measurements (see section 3.2, main text).

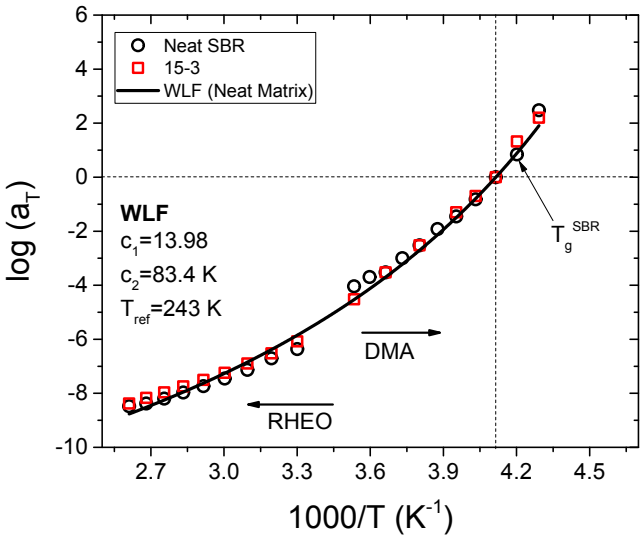

Figure S2: Dynamic map resulting in the mastercurves building for the Neat SBR and the 15-3 sample for comparison. The reference temperature was set to -30 °C, similarly as in Figure 3 (main text). The high and low temperature sets of data correspond respectively to the rheology and DMA experiments.

3. Additional DSC test on a SBR-PPG mixture

In Figure S3, we present a DSC experiment showing that a mixture of PPG and SBR presents two glass transitions when its composition is set to 21% PPG and 79%SBR, i.e. close to the polymer phase composition in the 15-8 sample (see Table 1). This result was not necessarily expected since the solubility parameters of the two polymers are very close to each other, it shows therefore that these indicators might be misleading and that one should rather consider the three components of the Hildebrand parameter (as well illustrated in the literature: ***dispersion***, ***polar*** and ***hydrogen bonding*** components).

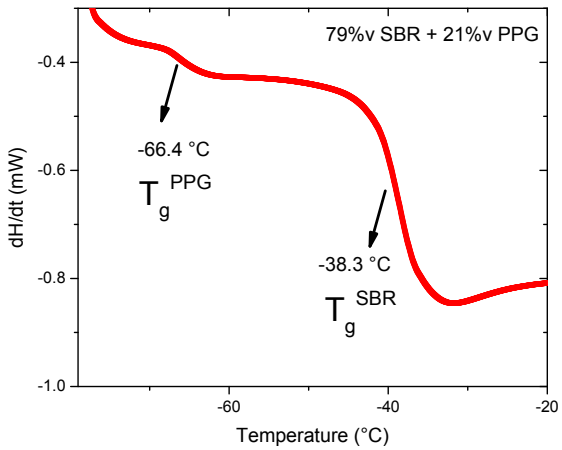

Figure S3: DSC experiment performed on a mixture of PPG (21%v) and SBR (79%). The two glass transitions reveals the poor miscibility of the two components in spite of their similar Hildebrand parameter.

4. Complementary TEM characterization

For the sake of completeness we provide in Figures S4 the TEM micrographs obtained on the 15-1 and 15-5 samples. The experimental conditions are identical as for the pictures shown in Figure 5 (main text). Of a particular interest, one can remark the presence of white dots on the 15-5 sample, i.e., the beginning of the PPG phase separation at the silica/SBR interface. (The last stage is the formation of a true core-shell structure as in the 15-8 sample).

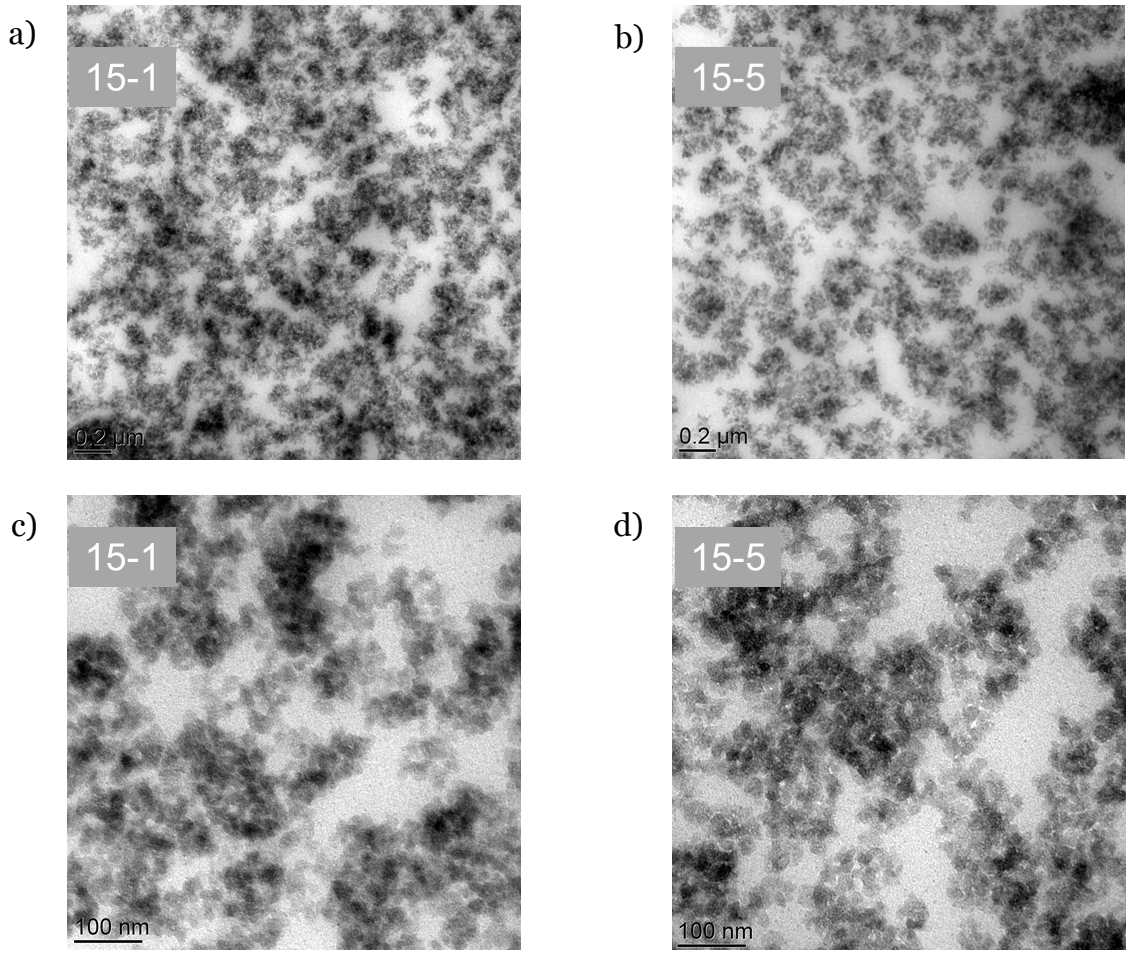

Figure S4: TEM micrographs. a-c) 15-1 sample, b-d) 15-5 sample. Figure d is of particular interest since it shows the presence of brighter dots in the black zones, i.e. the presence of PPG adsorbed at the silica/SBR interface.

5. Broadband Dielectric Spectroscopy (BDS)

We performed dielectric spectroscopy experiments on the two series of samples. This technique is widely used to study nanocomposites because it allows notably to probe dynamic heterogeneities likely to exist at the filler-polymer interface.[2, 3, 4] In addition, investigating the ionic conductivity σ_{DC} (at high temperature) provides important information regarding the filler structure, in particular in terms of percolation at which a jump in property is usually seen.[5]

As expected, varying the filler fraction (Figure S5a) dramatically changes the dielectric response of the material on the whole frequency range. Adding silica (5 vol.%) makes emerge an interfacial diffusion process (Maxwell-Wagner Sillar, "MWS") and diminishes the ionic conductivity because of charge carriers trapping. At higher silica content (15 vol.%), a hard (percolated) network is formed offering to the ions a much higher mobility, leading to an enhanced ionic conductivity. Finally, increasing the concentration in PPG (Figure S5b) is found to have almost no impact on the dielectric properties, in good agreement with an invariant silica structure as observed with both microscopy and scattering techniques.

a)

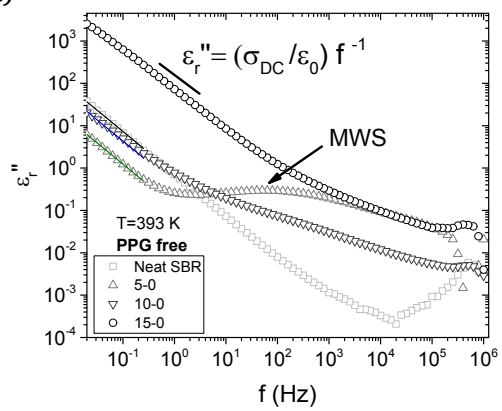

b)

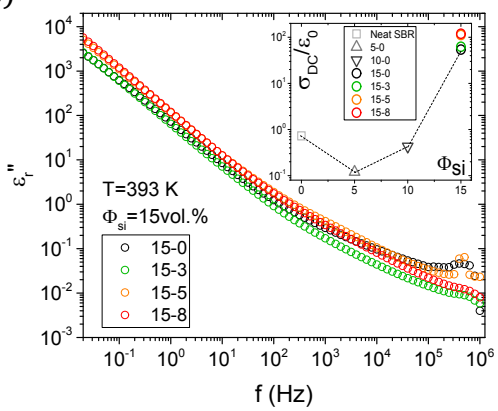

Figure S5: Dielectric properties of the nanocomposites and the corresponding neat SBR varying a) the silica content and b) the PPG concentration. Inset: Normalized ionic conductivity as a function of the filler fraction and PPG concentration.

Broadband Dielectric Spectroscopy (BDS) : Methods

Broadband dielectric spectroscopy experiments were conducted on a Modulab MTS System device (Solartron Analytical, United Kingdom) at constant temperature T=120 °C allowing the extraction of the ionic conductivity. (Relaxation modes seen at lower temperatures are not treated in the article). The measurement cell consisted in 2 mm thick disk-like samples having a diameter of 20 mm sandwiched in-between two gold-plated electrodes. Prior to the measurements, samples were first annealed for 15 minutes at 140 °C for evaporating the residual water and relaxing eventual internal stress. The relative complex permittivity was then measured from 10^5 to 10^{-2} Hz under a static Helium atmosphere providing a temperature control better than 0.1 K.

6. Kraus Model (fitting strain sweep measurements)

In this section we present the data fitting of the storage modulus $G(\gamma)$ that we obtained in Figure 6 with the help of the Kraus model (see below).[6]

$$\frac{G'(\gamma) - G'_{inf}}{G'_0 - G'_{inf}} = \frac{1}{1 + \left(\frac{\gamma}{\gamma_c}\right)^{2m}}$$

Although this approach is purely empirical, it allows extracting trends regarding the different parameters of the model such as the critical deformation γ_c (transition between the linear and non-linear regimes) or the exponent m, related with the "steepness" of the modulus fall in the non-linear regime. Besides, note that this approach is not adapted to fit the corresponding loss moduli $G''(\gamma)$, revealing here again its empirical character.

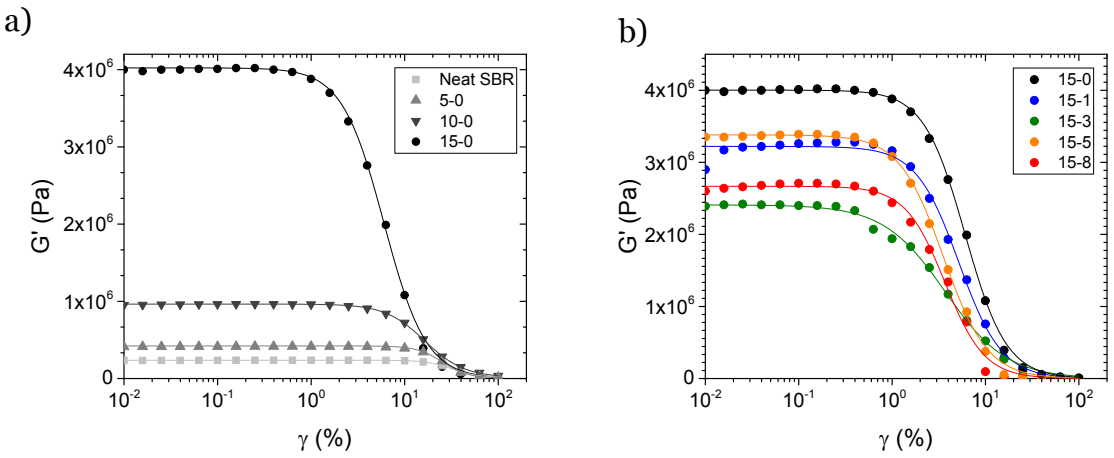

Figure S6: Lin-Log representation of the strain sweep measurements presented in the manuscript in Figure 6. The solid lines are fit to the data with the Kraus model. The fit parameters are reported in the Table SX. a) Free PPG samples with increasing the fraction in silica, b) nanocomposites loaded with 15 vol.% and various amount of PPG.

Table S1: Kraus model fit parameters extracted for $G'(\gamma)$

Sample	G_{inf}' **(Pa)**	G_0' **(Pa)**	γ_c **(%)**	m **(-)**
Neat SBR	1.5 10^4	2.3 10^5	31.9	1.59
5-0	4.3 10^3	4.2 10^5	25.3	1.58
10-0	1.4 10^4	9.4 10^5	16.4	1.03
15-0	1.0 10^3	4.0 10^6	6.0	0.97
15-1	1.0 10^3	3.2 10^6	5.2	0.95
15-3	1.0 10^3	2.4 10^6	3.7	0.66
15-5	1.0 10^3	3.4 10^6	3.7	0.92
15-8	1.0 10^3	2.7 10^6	3.6	1.02

Numbers in red stand for the fitting procedure limits (putting $G_{inf}' = 0$ would result in a similar fit).

Note that this empirical approach allows highlighting the reduction of the linear regime and the steepening of the storage modulus fall at high deformation when the silica content is increased (both γ_c and m decrease when Φ_{si} is enhanced). These results are well known and are generally included in the so-called Payne Effect.

Apart from this result, empirical models cannot make a clear difference in terms of fit parameter or physical meaning when the PPG content is varied. Indeed, all the parameters vary in a hieratic way making difficult a physical interpretation beyond the

softening of the material (as proposed in the manuscript). Deeper analyses will be eventually proposed in the future.

7. Reproducibility of the tensile tests – Error bars

In order to have a robust idea on the failure points, we repeated the tensile tests presented in Figure 9 (main text) at least three times. The error bars on the stress and strain at the failure point are provided in Figure S7. These results show that the amplitude of the error bar is increasing with the volume fraction in silica whereas it seems to be independent on the PPG concentration. A particular attention can be paid on the 15-8 sample which shows a significantly lower elongation at rupture. We believe that this effect is most likely related with the presence of large "unbroken" agglomerates (Figure 5d) caused by the too low torque recorded during the mixing procedure (Figure 1c).

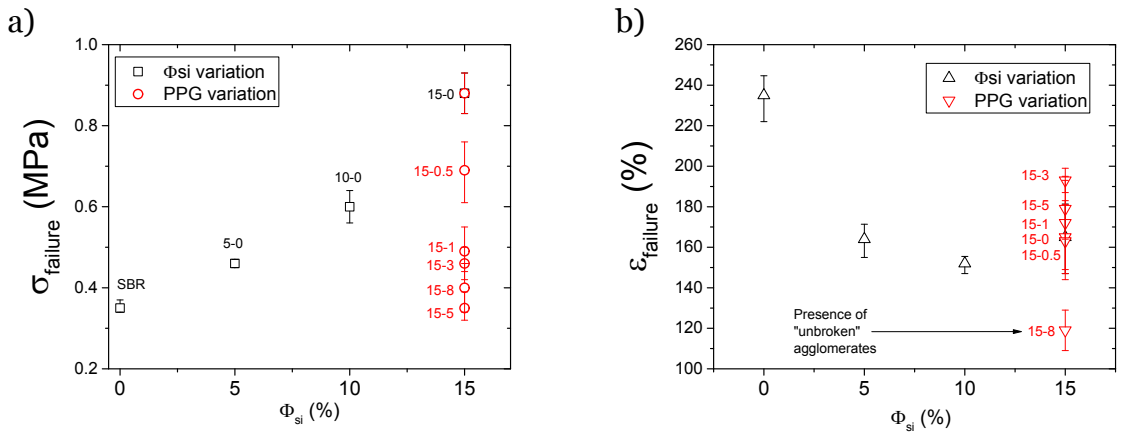

Figure S7: Error bars on the coordinates of the failure point measured through tensile test for the whole set of samples. At least three tests are used to build the error bars (maximum – average – minimum). a) True stress, b) True strain.

8. "Forward" and "Backward" strain sweeps experiments.

In addition to the DSS tests provided in Figure 7, we performed similar strain sweeps recording both the properties increasing and decreasing the strain amplitude (respectively called "forward" (*f*) and "backward" (*b*)). These experiments are shown in Figure S8 where we increased the deformation from 0.002% up to 400% (G'_f, G''_f), before to come back progressively to 0.002% (G'_b, G''_b).

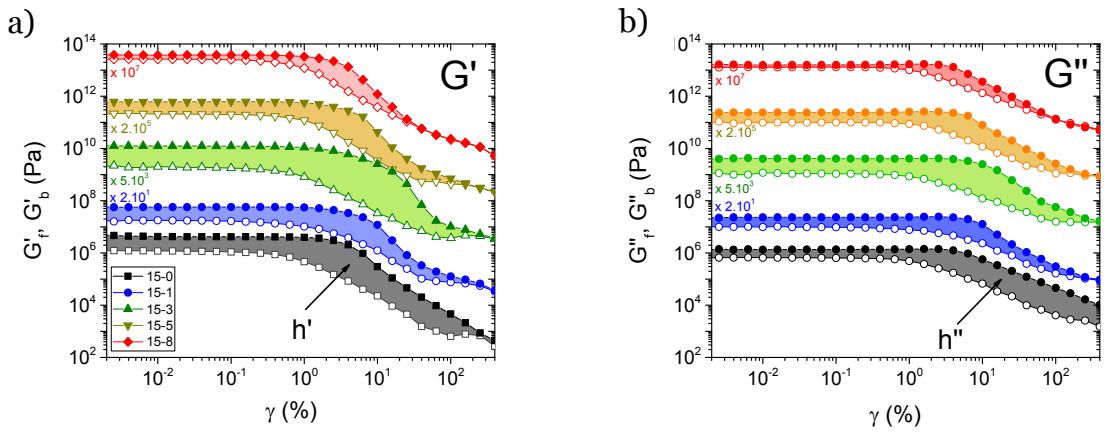

Figure S8: Dynamic strain sweep experiments performed on the nanocomposites loaded with 15 vol.% in silica and various fraction of PPG. The amplitude is first increased from 0.002% to 400% before to be decreased back to the same point. The frequency and the temperature are respectively set to 1 rad.s^{-1} and 110 °C. The colored zones represent the hysteresis of the material. Data have been shifted for clarity. a) G' and b) G''.

The hysteresis of the material is defined as $h^i = \int_{\gamma_{max}}^{\gamma_{max}} G_f^i - G_b^i \, d\gamma$. Here, the exponent "i" stands for the storage (') or the loss ('') contribution. The evolution of h^i with the

volume fraction in PPG is plotted in Figure S9, where it is clearly seen to decrease, suggesting an earlier "reconstruction" of the aggregates' network, in good agreement with the idea of the lubrication conferring higher coefficient of diffusion to the filling objects. This effect is particularly visible at high strain (Figure S8) where G'_f and G'_b overlap for the 15-8 sample (red) whereas they are very different in 15-0 (black).

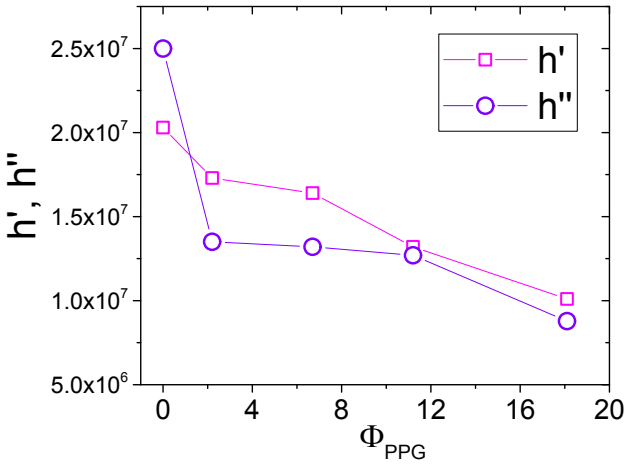

Figure S9: Storage h' and loss h'' moduli hysteresis as a function of the volume fraction in PPG.

Lastly we present in Figure S10 three dynamic strain sweep tests performed on the 15-3 sample showing the good reproducibility of our data (G' and G''), far in the non-linear regime.

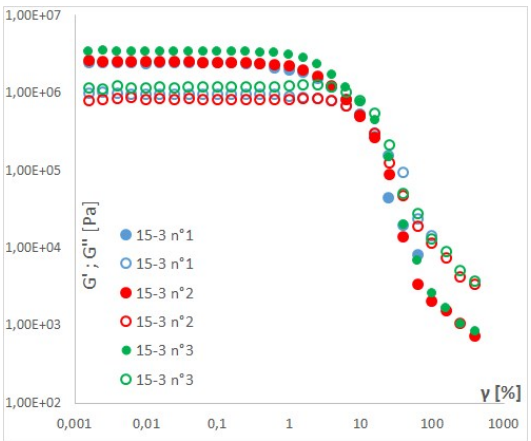

Figure S10: Three identical dynamic strain sweeps performed on the 15-3 sample showing the reproducibility of our measurements. The method is identical to the one used to measure the data in Figure 7 (main text) and in Figure S8.

References:

1. G. P. Baeza, A.-C. Genix, C. Degrandcourt, L. Petitjean, J. Gummel, M. Couty and J. Oberdisse, *Macromolecules*, 2013, **46**, 317-329.
2. G. P. Baeza, C. Dessi, S. Costanzo, D. Zhao, S. S. Gong, A. Alegria, R. H. Colby, M. Rubinstein, D. Vlassopoulos and S. K. Kumar, *Nat. Commun.*, 2016, **7**.
3. A. P. Holt, J. R. Sangoro, Y. Wang, A. L. Agapov and A. P. Sokolov, *Macromolecules*, 2013, **46**, 4168-4173.
4. A. P. Holt, P. J. Griffin, V. Bocharova, A. L. Agapov, A. E. Imel, M. D. Dadmun, J. R. Sangoro and A. P. Sokolov, *Macromolecules*, 2014, **47**, 1837-1843.
5. G. P. Baeza, J. Oberdisse, A. Alegria, K. Saalwächter, M. Couty and A.-C. Genix, *Polymer*, 2015, **73**, 131-138.
6. J.-C. Majesté, in *Rheology and Processing of Polymer Nanocomposites*, 2016.